BIODIVERSITAS
Volume 26, Number 6, June 2025
Pages: 2773-2785

ISSN: 1412-033X
E-ISSN: 2085-4722
DOI: 10.13057/biodiv/d260622

Decoding halophilic biofilm development across salinity gradients in hypersaline environments

ILHAM MISBAKUDIN AL ZAMZAMI[1], DEFRI YONA[2], ABD RAHEM FAQIH[3], ANDI KURNIAWAN[3,♥]

[1]Doctoral Program of Fisheries Science and Marine, Faculty of Marine Science and Fisheries, Universitas Brawijaya. Jl. Veteran, Malang 65145, East Java, Indonesia

[2]Department of Fishery and Marine Resources Utilization, Faculty of Marine Science and Fisheries, Universitas Brawijaya. Jl. Veteran, Malang 65145, East Java, Indonesia

[3]Department of Fisheries Marine Resources Management, Faculty of Marine Science and Fisheries, Universitas Brawijaya. Jl. Veteran, Malang 65145, East Java, Indonesia. Tel.: +62-341-553512, Fax.: +62-341-557837, ♥email: andi_k@ub.ac.id

Manuscript received: 21 April 2025. Revision accepted: 27 June 2025.

Abstract. *Al Zamzami IM, Yona D, Faqih AR, Kurniawan A. 2025. Decoding halophilic biofilm development across salinity gradients in hypersaline environments. Biodiversitas 26: 2773-2785.* Halophilic microorganisms possess distinctive adaptations that enable survival and biofilm formation under extreme salinity, exhibiting considerable promise for biotechnological applications. However, halophilic biofilms' structural and biochemical properties across varying salinity gradients remain insufficiently characterized. The present study investigates the biofilm formation on High-Density Polyethylene (HDPE) substrates in NaCl concentrations ranging from 2% to 40% over 21 days. A multidisciplinary approach was employed to characterize biofilm development and microbial responses. This approach included metagenomics, Confocal Laser Scanning Microscopy (CLSM), Fourier-Transform Infrared Spectroscopy (FTIR), and water quality analyses. The results demonstrated that optimal biofilm formation occurred at 20% NaCl, exhibiting peak microbial abundance, biovolume, protein content, and metabolic activity, accompanied by increased acid production, decreased pH, and reduced dissolved oxygen. Conversely, 40% NaCl elicited a substantial response characterized by severe osmotic stress, a marked deterioration in cell viability and biofilm integrity, and a notable elevation in turbidity consequent to cellular damage. Biofilms at 2% NaCl were stable but exhibited reduced metabolic activity and simpler structures. These results highlight the adaptive capacity of halophilic biofilms, especially at moderate salinities, providing essential insights into their ecological roles and applications in saline wastewater treatment and sustainable environmental management.

Keywords: Bacteria, biofilm, halotolerant, metagenomics, microbial ecology

INTRODUCTION

Biofilms, structured communities of microorganisms adhered to surfaces, are embedded within an Extracellular Polymeric Substance (EPS) matrix primarily composed of polysaccharides, proteins, and nucleic acids (Mahto et al. 2022; Kurniawan and Fukuda 2023). The biotechnology field has recently focused intensely on biofilms, given their distinctive structural characteristics and functional adaptability. These surface-associated microbial communities, embedded in a self-produced extracellular matrix, demonstrate remarkable environmental resilience and stress resistance (Gonzalez-Machado et al. 2018; Wang et al. 2023). These organisms' adaptability has enabled various applications, including wastewater treatment, bioremediation, and biochemical production (Ulinuha et al. 2020; Nurfitriani et al. 2022). Beyond functioning as microbial aggregates, biofilms enhance production efficiency in bioconversion processes through their optimized structure and dynamics (Basotra et al. 2022). The EPS matrix confers protection to biofilm communities against environmental stressors, including extreme temperature fluctuations, desiccation, chemical agents, and antibiotics, thereby enhancing microbial resilience (Rath et al. 2022; Kurniawan et al. 2024c). In hypersaline environments, biofilms provide essential habitats for halophilic microorganisms adapted to high salinity conditions (Anggayasti et al. 2025).

Halophilic bacteria have been observed to thrive in high-salt environments, including seawater, solar salterns or salt ponds, salt lakes, and salt mines. The classification of halophiles is based on their salt requirements, which can be divided into slight, moderate, or extreme categories (Orhan and Demirci 2020; Citarasu et al. 2021). These organisms have been observed to exhibit diverse biochemical adaptations in response to their environment. Solar salterns exhibit salinity gradients that give rise to distinct microhabitats, supporting various microbial communities, including haloarchaea (Basotra et al. 2022; Al Zamzami et al. 2023b). These organisms maintain osmotic balance through compatible solute synthesis and salt-tolerant proteins (Oren 2015; Naamala et al. 2023). A prevalent strategy employed by these organisms is the salt-in approach, which involves the accumulation of intracellular ions. This process serves to prevent desiccation and maintain metabolic function. Their stratified communities exhibit moderate halophiles in lower salinity ponds and extremophiles in hypersaline crystallizers (Thompson et al. 2022; Tat 2024). This environmental gradient significantly influences nutrient cycling, thereby yielding industrially valuable compounds. Salterns function as natural laboratories for studying

halophilic adaptations while concurrently offering biotechnological potential through their unique enzymes and metabolites (Al Zamzami et al. 2023a). Nevertheless, most current research has emphasized individual planktonic halophilic strains, leaving the structural and functional aspects of halophilic biofilms significantly understudied.

A critical knowledge gap persists regarding the mechanisms underlying halophilic biofilm formation and persistence, particularly when utilizing natural salt pond water under varying salinities. The complexity of biofilm communities, microbial interactions, and EPS structural compositions remains insufficiently characterized in these settings. Moreover, the contributions of biofilms to overall biodiversity and ecosystem stability in hypersaline environments require further exploration.

To address these gaps, this study investigates the characteristics of halophilic biofilms developed under varying salinity levels (2%, 20%, and 40% NaCl) using water collected from salt ponds. A comprehensive, multi-method approach is employed, integrating metagenomic analysis, Confocal Laser Scanning Microscopy (CLSM), Fourier-Transform Infrared Spectroscopy (FTIR), protein profiling, and Total Plate Count (TPC) to examine the biofilm's structural integrity, microbial composition, and viability. Concurrently, environmental parameters (i.e., pH, dissolved oxygen, turbidity, conductivity, and total dissolved solids) are systematically monitored to assess their impact on biofilm dynamics.

The novelty of this study lies in its integrative analytical framework, which enables a detailed characterization of halophilic biofilms within real-world hypersaline settings. By identifying the salinity conditions most conducive to robust biofilm development and clarifying the associated structural and functional attributes, the findings offer valuable insights into the ecological significance of halophilic biofilms and their potential for biotechnological innovations, particularly in saline wastewater treatment, salt production, and sustainable environmental applications.

MATERIALS AND METHODS

Experiment design

The initial step involved preparing water samples with 2%, 20%, and 40% salinity levels collected from salt ponds on the South Coast of Malang District, Indonesia. Salinity was measured using a Smart Salt Detector (SD-B01071, Matra Indonesia). These specific salinity levels correspond to different stages of salt production: 2% represents initial seawater evaporation, 20% is the crystallization stage, and 40% represents bittern, a high-salinity byproduct (Kurniawan et al. 2019; Kurniawan et al. 2024a). Next, the water samples with different salinities were placed into separate 10-liter aquariums containing High-Density Polyethylene (HDPE) substrates sized 15 × 10 cm, secured with stainless steel weights. HDPE was selected as it is commonly used in Indonesian salt ponds. Biofilm formation was observed over 21 days, consistent with the typical biofilm maturation timeframe (Kurniawan and Fukuda 2023). After the growth period, biofilms were sampled by gently brushing the HDPE surface in one direction while rinsing with 40 mL of distilled water. The harvested biofilm was homogenized and divided for subsequent analyses. Additionally, water samples from each aquarium were collected on days 0 and 21 for total bacterial number with Total Plate Count (TPC) assessments. Each experimental setup was conducted in triplicate to ensure data reliability.

Metagenomic analysis

Metagenomic analysis was conducted to identify bacterial community composition within biofilms. Due to limited sample volume, biofilms from all salinity treatments (2%, 20%, and 40%) were pooled. PCR amplification of the target regions was conducted using barcode-linked specific primers. PCR products of the correct size were isolated via 2% agarose gel electrophoresis. An equal quantity of PCR products from each sample was pooled, followed by end repair, A-tailing, and ligation with Illumina adapters. The libraries were then sequenced on an Illumina paired-end platform, producing 250-bp paired-end raw reads. Prior to sequencing, library quality was assessed using Qubit for quantification, real-time PCR for validation, and a bioanalyzer for size distribution analysis. The quantified libraries were pooled and sequenced on Illumina platforms based on library concentration and required data volume. The metagenomic analysis targeted the V3-V4 region (470 bp) using primers 341F (5'-CCTAYGGGRBGCASCAG-3') and 806R (5'-GGACTACNNGGGTATCTAAT-3') (Thompson et al. 2022). Sequence analyses were performed using Uparse software (v7.0.1090), clustering sequences into Operational Taxonomic Units (OTUs) at 97% similarity. Representative sequences from each OTU underwent taxonomic annotation against the SILVA138 SSUrRNA database via the Qiime-Mothur method. MUSCLE software (Version 3.8.31) was employed for phylogenetic analysis. The Krona visualization process involves three key steps: (i) taxonomic classification of FASTQ data using Kraken2, (ii) conversion of classification results to Krona format, and (iii) generation of interactive diagrams via the ktImportTaxonomy command. This pipeline produces interactive graphical representations of microbial composition accessible through web browsers, enabling intuitive analysis of microbial communities from domain to species level.

Confocal laser scanning microscopy

Confocal Laser Scanning Microscopy (CLSM) was used to analyze the viability and composition of live and dead cells in halophilic biofilms in real-time. In addition, this analysis was used to analyze the quantity of biofilm over 21 days. An analysis process using Confocal Laser Scanning Microscopy (CLSM) followed the method by Gonzalez-Machado et al. (2018) with modifications. Sample preparation was carried out by cutting HDPE covered with biofilm (1 × 1 cm^2). Cells were stained using the QIA76 Sigma-Aldrich Staining Kit (Cyto-dye Ex/Em: 488/518, PI Ex/Em: 488/615) to determine live or dead cells. Then, the HDPE was rinsed gently with a staining buffer and dripped with 10 µL of Cyto and PI dye. Next, incubate the HDPE in the dark at room temperature (27-28°C) for 30 minutes.

After incubation, HDPE was observed under a microscope (OLYMPUS FV-1000, Japan).

Protein staining of biofilm was done using another HDPE with a size of 1 × 1 cm with FITC 46950 Sigma-Aldrich (Ex/Em: 492/518). The HDPE was rinsed slowly using 0.1 M phosphate buffer and then dripped with 10 µL of FITC Dye. Next, incubate the HDPE in the dark at room temperature (27-28°C) for 30 minutes. After incubation, HDPE was observed under a microscope (OLYMPUS FV-1000, Japan).

Fourier transform infrared

FTIR analysis was conducted to determine the chemical composition of halophilic biofilms. Biofilm samples were centrifuged at 1500 rpm for 5 minutes using a Flexyfuge C1000 (Argos Technologies, China). The resulting pellets were dried at 60°C for 24 hours in an SLI-220 oven (Eyela Tokyo, Japan). Dried biofilm pellets were thoroughly mixed with Potassium Bromide (KBr) in a 1:10 ratio (Gieroba et al. 2023). The prepared samples underwent infrared scanning using a Shimadzu IR Prestige 21 (Japan) within a 4000-450 cm^{-1} wavelength range.

Total plate count

Total Plate Count (TPC) was performed to assess bacterial abundance in initial water samples (D0), final water samples (D21), and biofilms at three salinity levels (2%, 20%, 40% NaCl). Plate Count Agar (17.5 g) and respective amounts of NaCl (2 g, 20 g, or 40 g) were dissolved in 1000 mL distilled water, homogenized, and sterilized at 121°C for 15 minutes. The sterile medium was poured into petri dishes and allowed to solidify. Each petri dish received 1 mL of sample (water or biofilm), spread evenly using a sterile hockey stick. After 24 hours of incubation, bacterial colonies were counted for 7 days, and bacterial abundance was calculated according to SNI 2332.3:2015 as follows:

$$\text{Total bacteria (CFU/mL)} = \frac{1}{\text{dilution factor}} + \text{number of colony} \quad (1)$$

Measurement of water quality

Water quality measurements were carried out during the experiment (21 days) to analyze water quality dynamics. Water quality parameters included temperature, dissolved oxygen, turbidity, conductivity, and pH using a Water Quality Checker (WQC-22A, DKK TOA Corporation, Japan). TDS was measured using a TDS meter (Lutron YK22CTA, USA).

RESULTS AND DISCUSSION

Metagenomic analysis of biofilm communities

The krona plot visually represents the taxonomic annotation results, displaying different taxonomic ranks as concentric circles from the center outward. The area of each sector reflects the relative proportion of annotated OTUs for various taxa. Sequencing results demonstrated high-quality data with an average of 160,491 total tags representing sequencing depth, including 158,871 taxon tags (99% classification rate) successfully assigned to known taxonomic groups, 15 unclassified tags indicating minimal unassigned sequences, 1,605 unique tags reflecting sequence diversity, and 196 Operational Taxonomic Units (OTUs) suggesting moderate microbial diversity within the biofilm community. The krona visualization of the halophilic biofilm (Figure 1) highlights the taxonomic distribution across all domains.

The krona plot reveals two major domains identified in the biofilm: Bacteria (99%) and Archaea (0.7%), with a small fraction (0.1%) unclassified. The dominance of the Bacteria domain indicates that bacterial taxa are the most abundant within the hypersaline biofilm. Bacterial dominance can be attributed to the broad halotolerance observed across many bacterial species, which enables them to survive in high-salinity environments. Bacterial communities exhibit universal resilience due to rapid genetic adaptability, allowing them to thrive under diverse conditions, including hypersaline habitats (Wang et al. 2022). This finding contrasts with research by Rieder et al. (2023), which characterized the microbial composition of biofilms in a Recirculating Aquaculture System (RAS) using 16S rRNA gene sequencing, revealing an exclusively bacterial community (100% relative abundance) with no detectable archaeal taxa.

Although archaea are known for their ability to endure extreme environments such as salt ponds, where high salinity prevails, their abundance is significantly lower than that of bacteria. The presence of archaea at 0.7% suggests that while they contribute to the community, their role is less prominent than that of bacteria. Most archaea fall under the extremophile category, inherently resisting harsh conditions (Shu and Huang 2022). Nevertheless, the higher abundance of bacteria indicates their more extensive adaptation strategies and metabolic diversity, which enable them to exploit various nutrient sources available in hypersaline environments, such as organic matter from other organisms or metabolic byproducts (Jurdzinski et al. 2023).

Several halophilic bacteria from the Bacteria domain have evolved efficient osmoregulatory mechanisms, allowing them to cope with saline conditions. Additionally, bacteria's broader metabolic versatility compared to archaea provides a competitive advantage in utilizing different nutrient sources. These capabilities may also allow bacteria to form symbiotic or competitive interactions with other organisms, enhancing their survival and proliferation in hypersaline ecosystems. In contrast, such interactions may be less developed in archaea within this environment, potentially limiting their abundance. Halophilic bacteria consistently outcompete archaea in moderately hypersaline ecosystems (10-25% NaCl) due to their superior osmoregulatory plasticity, broader metabolic versatility, and complex symbiotic networks. While both domains employ osmoadaptation strategies, bacteria possess more diverse compatible solute systems and can utilize a wider range of organic substrates, enabling them to dominate nutrient cycling. Archaea, though highly specialized for extreme salinity (>30% NaCl), are generally restricted to narrower niches and lack equivalent capacities for interspecies

cooperation (Thompson et al. 2022). This functional divergence explains why bacterial taxa typically comprise >90% of hypersaline biofilm communities, with archaeal representation rarely exceeding 5% except in saturated brines or anoxic zones where their unique adaptations prove advantageous (Sauer et al. 2022).

Krona visualization of the Bacteria domain

The krona visualization for the Bacteria domain (Figure 2) provides insights into the composition and relative abundance of different bacterial genera within the halophilic biofilm. Among the identified genera, *Limimaricola* (39%) and *Bacillus* (30%) emerged as the most dominant, representing the major bacterial community in the biofilm.

Limimaricola, a genus known for mild halophilicity, consists of species that generally require NaCl for growth, with optimal conditions typically found at 25-30°C, 2-3% (w/v) NaCl, and pH 7.0 (Lyu et al. 2022). The ability of Limimaricola species to metabolize a wide range of organic carbon compounds makes them well-suited for colonization and biofilm formation in hypersaline environments (Ding et al. 2022). Their dominance in the biofilm aligns with previous findings, where species from this genus have been isolated from various marine biofilms, sediments, beach sands, and seawater (Jurdzinski et al. 2023). The prevalence of *Limimaricola* suggests that they play a significant role in the structural and functional dynamics of the biofilm, possibly by utilizing diverse organic substrates available in the environment.

Bacillus, another predominant genus, includes several species with halotolerant characteristics, allowing them to survive and thrive under varying salinity levels. Halotolerant *Bacillus* species, such as *Bacillus horikoshii* (Orhan and Demirci 2020), *Bacillus selenatarsenatis* (Wang et al. 2022), and *Bacillus beringensis* (Sarwa et al. 2024), have been re-ported to adapt to different salt concentrations. This adaptability is facilitated by mechanisms such as efficient osmoregulation and the production of compatible solutes, which help maintain cellular stability under osmotic stress. The significant presence of Bacillus in the biofilm indicates its ecological versatility and ability to colonize hyper-saline environments effectively.

The krona plot further reveals that approximately 37 bacterial genera are present within the biofilm, suggesting a diverse and complex microbial community. This diversity indicates the biofilm's ability to harbor a variety of metabolic functions and ecological interactions, potentially including nutrient cycling, organic matter degradation, and symbiotic relationships (Perwira et al. 2020). The coexistence of multiple genera with varying degrees of halotolerance and metabolic capabilities likely contributes to the resilience and stability of the biofilm in hyper-saline conditions.

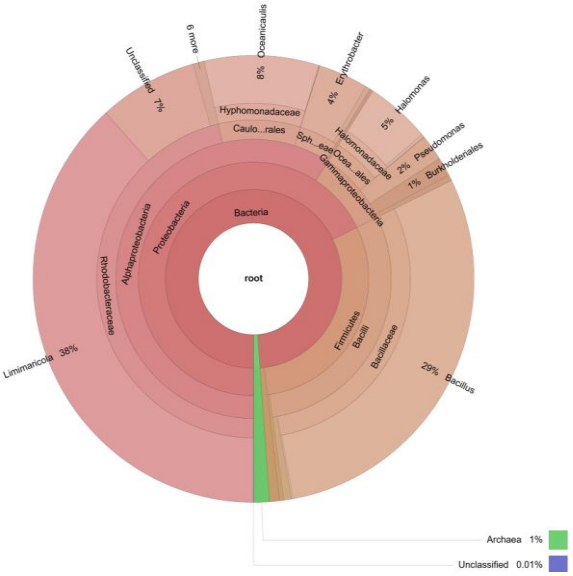

Figure 1. Krona chart of all domains (Archaea and Bacteria) in the biofilm

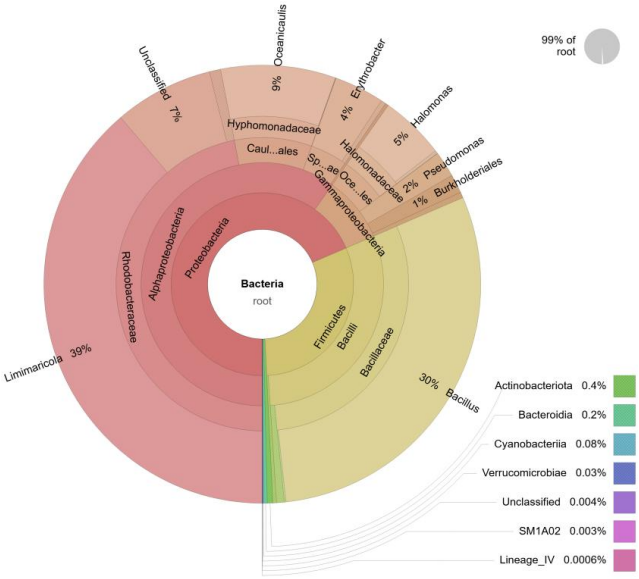

Figure 2. Krona chart of bacteria in the biofilm

Krona visualization of the Archaea domain

The krona plot for the Archaea domain (Figure 3) displays the taxonomic distribution of archaeal genera in the biofilm. The results show that the genus *Halohasta* (65%) dominates the community, followed by *Haloarcula* (16%). In total, approximately 11 genera were identified, including *Haloferax* (3%), *Halobacterium* (2%), *Halolamina* (1%), *Halomicrobium* (3%), *Halosimplex* (1%), and smaller proportions of other genera such as *Halogeometricum*, *Halogranum*, *Haloplanus*, and *Nanohaloarchaeota*. A small fraction (5%) of unclassified genera indicates that some archaeal taxa remain unidentified.

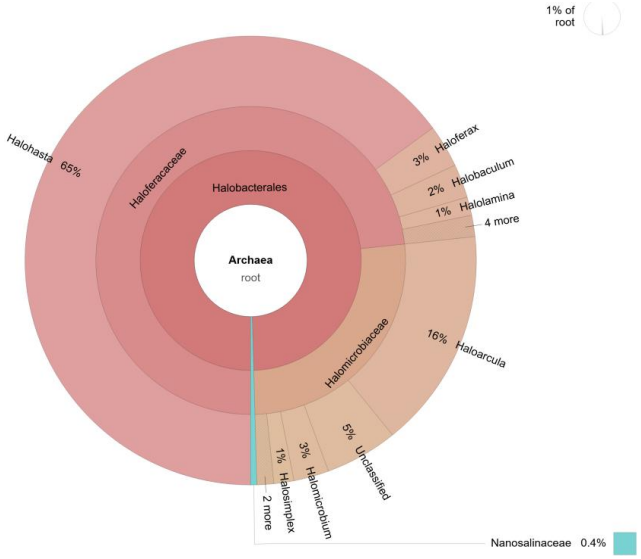

Figure 3. Krona chart of archaea in the biofilm

Halohasta, classified as an extreme halophile, is known for its ability to thrive in highly saline environments such as the Dead Sea, Great Salt Lake, and salt ponds (Oren 2015; Thompson et al. 2022). The dominance of Halohasta in the biofilm suggests its significant role in maintaining the stability and resilience of microbial communities under hypersaline conditions. The genus's adaptations, such as specialized ion pumps and protective membrane structures, enable it to cope with high osmotic stress, which is essential for survival in environments with salinity exceeding that of seawater.

Haloarcula, which constitutes 16% of the archaeal community, is also a well-known extreme halophile. It shares adaptive features with *Halohasta*, including osmoregulation and salt tolerance mechanisms. The presence of other genera, albeit in lower proportions, indicates a diverse but specialized archaeal community well-adapted to high-salt conditions. The ability of these genera to form biofilms may enhance their survival by creating microenvironments that mitigate osmotic stress and facilitate nutrient exchange (Al-Daghistani et al. 2024; Sarwa et al. 2024).

The relatively lower abundance of genera such as *Halogeometricum*, *Halogranum*, and *Haloplanus* might be due to niche specialization or competitive exclusion by more dominant genera like *Halohasta*. However, their presence still contributes to the overall diversity and functionality of the biofilm, potentially playing roles in specific metabolic processes or stress responses. The significant proportion of unclassified archaea (5%) suggests that further exploration of the archaeal community could reveal novel or poorly understood taxa, which may possess unique adaptations for hypersaline environments. It underscores the need for continuous development of reference databases to improve the accuracy of taxonomic classification in metagenomic studies.

Integrating bacterial and archaeal data provides a comprehensive understanding of the biofilm community structure, where bacterial genera dominate in abundance and functional diversity. Meanwhile, the presence of archaea, though less abundant, adds to the resilience and adaptability of the biofilm, particularly under extreme salinity conditions. Current evidence suggests halophilic archaea may function as biofilm stabilizers under hypersaline conditions. Their unique adaptations, including EPS production and ion-regulation mechanisms, could provide structural integrity to the biofilm matrix while mitigating osmotic stress (Thompson et al. 2022). These findings suggest that while bacteria may be the primary contributors to biofilm dynamics in hypersaline environments, archaea play essential supporting roles that enhance the biofilm's overall ecological stability and functional capacity.

Phylogenetic analysis of the Top 10 genera

The phylogenetic analysis revealed the top 10 dominant genera in halophilic biofilms, with *Limimaricola* (38.32%) and *Bacillus* (29.40%) being the most abundant (Figure 4). These genera, along with *Oceanicaulis*, *Halomonas*, *Erythrobacter*, *Pseudomonas*, *Halohasta*, *Paraburkholderia*, *Roseivivax*, and *Methylotenera*, belong to the phyla Proteobacteria, Firmicutes, and Halobacterota, indicating a phylogenetically diverse microbial community adapted to hypersaline environments.

Limimaricola, from Proteobacteria, is mildly halophilic and capable of utilizing various organic carbon sources, playing a crucial role in organic matter degradation and nutrient cycling. *Bacillus* (Firmicutes) includes halotolerant species that survive under high salinity via osmoregulatory mechanisms and the production of compatible solutes. *Oceanicaulis* contributes to biofilm attachment and structure, while *Halomonas* is known for its extreme halotolerance and broad metabolic capabilities, enhancing the biofilm's resistance to osmotic stress.

The phylogenetic tree shows that genera such as *Limimaricola*, *Oceanicaulis*, and *Erythrobacter* cluster under Alphaproteobacteria, suggesting shared ecological roles. *Bacillus* forms a distinct branch, reflecting its unique adaptations to saline conditions. Although *Halohasta*, an archaeal genus, has a lower abundance, it plays a key role in stabilizing the biofilm under extreme salinity. This phylogenetic diversity reflects the biofilm's ability to support various metabolic processes and stress responses, enhancing its resilience in hypersaline conditions.

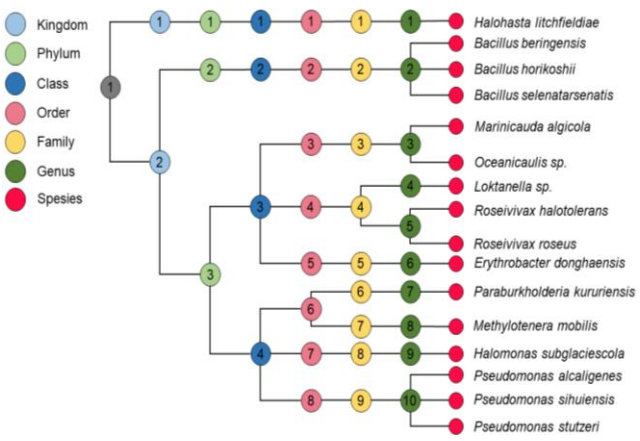

Figure 4. Phylogeny of the top 10 dominant genera

Table 1. Phylogeny of the top 10 dominant genera

Kingdom	Phylum	Class	Order	Family	Genus
Archae	Halobacterota	Halobacteria	Halobacterales	Haloferacaceae	*Halohasta*
Bacteria	Firmicutes	Bacilli	Bacillales	Bacillaceae	*Bacillus*
	Proteobacteria	Alphaproteobacteria	Caulobacterales	Hyphomonadaceae	*Oceanicaulis*
			Rhodobacterales	Rhodobacteraceae	*Limimaricola*
					Roseivivax
			Sphingomonadales	Sphingomonadaceae	*Erythrobacter*
		Gammaproteobacteria	Burkholderiales	Burkholderiaceae	*Paraburkholderia*
				Methylophilaceae	*Methylotenera*
			Oceanospirillales	Halomonadaceae	*Halomonas*
			Pseudomonadales	Pseudomonadaceae	*Pseudomonas*

Biofilm resilience in hypersaline conditions originated from its phylogenetic diversity, enabling metabolic versatility; different microbes perform complementary functions (e.g., oxygenic and anoxic processes simultaneously) and share stress-resistance resources (such as ectoine), creating a collective survival system that single species could not achieve (Sauer et al. 2022). These findings highlight the potential use of halophilic biofilms in biotechnological applications such as saline wastewater treatment and halotolerant enzyme production.

SEM analysis of biofilm viability under different NaCl concentrations

The SEM analysis, combined with Confocal Laser Scanning Microscopy (CLSM), was utilized to observe the growth and viability of halophilic biofilms at varying NaCl concentrations (2%, 20%, and 40%). The live/dead cell staining visually represented cell viability, where green fluorescence indicated live cells and red fluorescence represented dead cells. The results showed a clear correlation between NaCl concentration and the viability of cells within the biofilm, as depicted in Table 1.

At 2% NaCl, the biofilm predominantly displayed green fluorescence, indicating a high proportion of live cells. The low red fluorescence suggested minimal cell death, which implies that the 2% NaCl condition was close to the optimal salinity for several mildly halophilic microorganisms. This condition allowed the cells to maintain balanced osmotic pressure with the external environment, resulting in minimal osmotic stress and higher cellular activity and proliferation (Al Zamzami et al. 2023a; Tat 2024). The dominance of live cells under this condition indicates that many microbes in the biofilm could actively metabolize and grow, contributing to the biofilm's structural development.

When the NaCl concentration increased to 20%, the intensity of green fluorescence decreased, while the red fluorescence increased. This shift suggested a higher proportion of dead cells than the 2% NaCl condition, although live cells still outnumbered the dead cells. The increased cell death at 20% NaCl indicates that the microbial community was subjected to greater osmotic stress, prompting the cells to adapt through mechanisms such as synthesizing compatible solutes for osmoregulation (Sauer et al. 2022; Naamala et al. 2023). Despite the increase in stress, many cells could survive and adapt, indicating that this concentration might be within the upper tolerance range for some halophilic bacteria in the biofilm.

At the highest concentration of 40% NaCl, there was a substantial reduction in green fluorescence and a corresponding increase in red fluorescence, indicating a significant decline in cell viability. The high proportion of dead cells suggested that the extreme osmotic stress at this concentration overwhelmed the microbial community's adaptive mechanisms, leading to increased cell death. The ability of some cells to persist may be attributed to specific adaptations in extreme halophiles. Still, the dominance of dead cells implies that the biofilm's overall integrity and function were compromised under these harsh conditions. Many cells likely experienced dehydration or membrane damage, as indicated by the predominance of red fluorescence (Wang et al. 2023; Tat 2024). The findings suggest that mild halophiles thrive at lower salinities (2%); however, extreme halophilic conditions (40% NaCl) harm most of the biofilm's microbial community. The ability of some cells to survive across these conditions highlights the biofilm's adaptive potential, but the overall trend points toward a decrease in community viability as osmotic stress intensifies.

Biovolume and protein distribution in biofilms under different NaCl concentrations

The results of biovolume and protein intensity measurements (Table 2) indicate that varying NaCl concentrations affect the structural and functional properties of the halophilic biofilms. The observed trends in biovolume, protein intensity, and distribution provide insights into the biofilm's adaptive mechanisms under osmotic stress.

At 2% NaCl, the biofilm exhibited a biovolume of 10 μm^3, with relatively moderate intensity and protein distribution. This salinity level allowed for favorable growth conditions for many mildly halophilic bacteria, which could maintain their metabolic activities and proliferate within the biofilm matrix. The uniform protein distribution suggested the active synthesis of Extracellular Polymeric Substances (EPS) and other proteins essential for biofilm stability. These results align with the SEM analysis from Table 2, which showed a predominance of live cells, indicating that the environment at 2% NaCl supported healthy biofilm development and cellular activity.

Table 2. Appearance of live/dead cells in the biofilm in different treatments

Treatment	Type of analysis		
	Live cell	**Dead cell**	**Live and dead cells**
2% NaCl	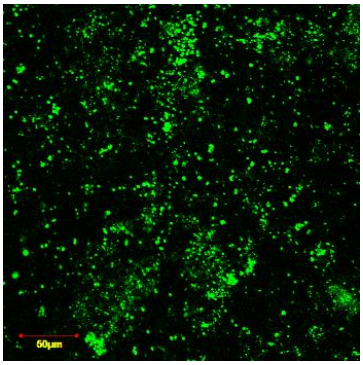	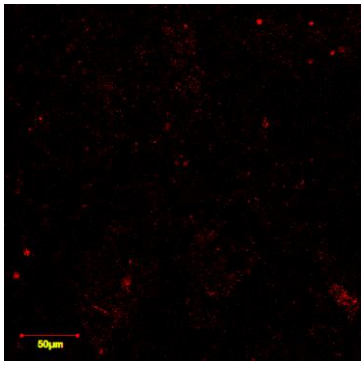	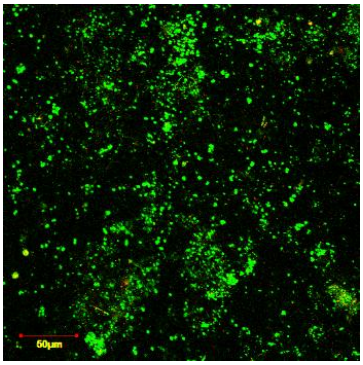
20% NaCl	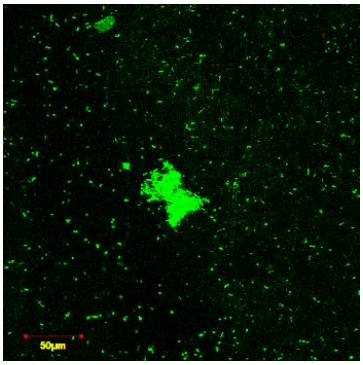	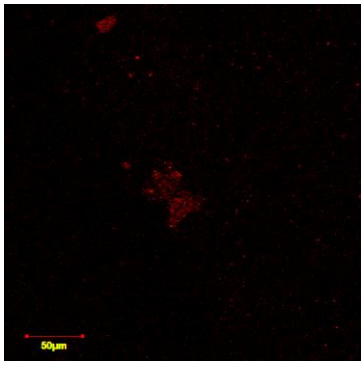	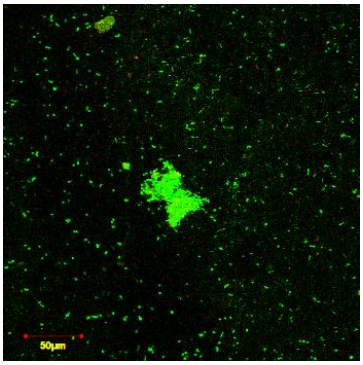
40% NaCl	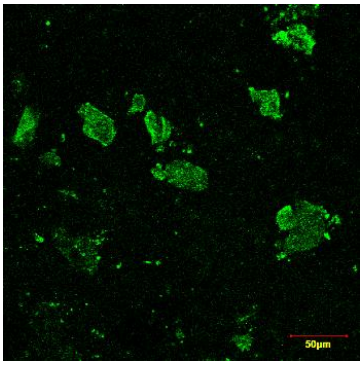	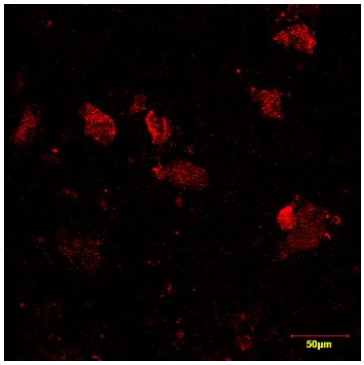	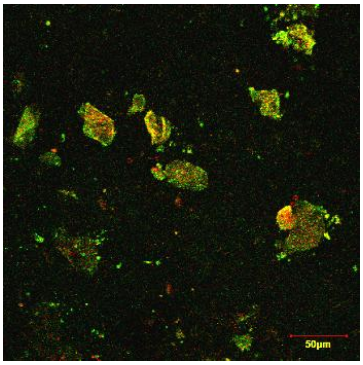

As the NaCl concentration increased to 20%, the biovolume rose to 18 µm³, reflecting an increase in biofilm density and possibly the thickness of the biofilm matrix. This increase in biovolume was accompanied by higher protein intensity and distribution, suggesting enhanced metabolic activity and EPS production. The greater biovolume and protein content at this salinity level indicates that the biofilm may have been reinforcing its matrix as a protective response to the higher osmotic stress. The heightened EPS production helps the microbial community mitigate osmotic stress by retaining water and stabilizing cellular structures. These adaptations are consistent with findings from previous studies, which show that increased biofilm production serves as a defense mechanism for bacteria under moderate osmotic stress (Sauer et al. 2022; Naamala et al. 2023). The SEM data in Table 2 also corroborated this, showing a slight increase in cell death, but many cells remained viable and active.

At 40% NaCl, there was a drastic reduction in biovolume to 5 µm³ and a marked decrease in protein intensity and distribution. This substantial decrease indicates that the extreme osmotic conditions at 40% NaCl were detrimental to the biofilm's structural integrity (Ulinuha et al. 2020; Tat 2024). The decrease in biovolume suggests a thinning of the biofilm matrix, potentially due to cell lysis or cell growth inhibition under severe osmotic stress. The low protein content further suggests that the biofilm's ability to produce EPS and other protective proteins was compromised at this salinity level. This reduction in biovolume and protein intensity correlates with the SEM findings in Table 2, which indicates a high proportion of dead cells, indicating that most of the biofilm's microbial community could not survive the extreme salinity. The high osmotic pressure likely disrupted cellular processes and membrane stability, leading to increased cell mortality (Sauer et al. 2022; Wang et al. 2023; Kurniawan et al. 2024b).

Table 3. Biovolume and protein intensity of biofilms grown at different NaCl levels

Treatment	Type of analysis		
	Biovolume (μm³)	Intensity	Protein
2% NaCl	10	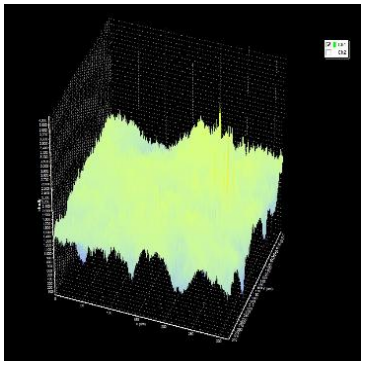	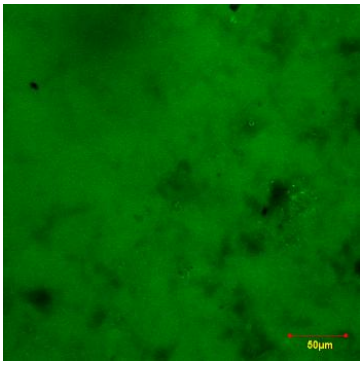
20% NaCl	18	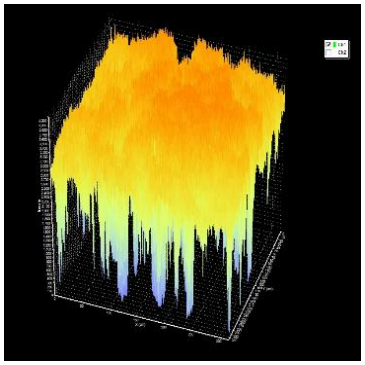	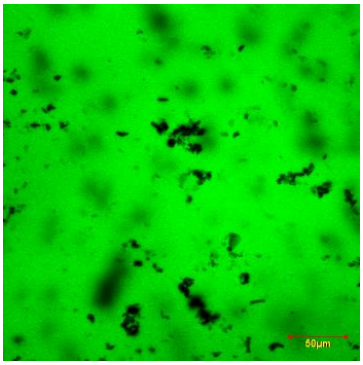
40% NaCl	5	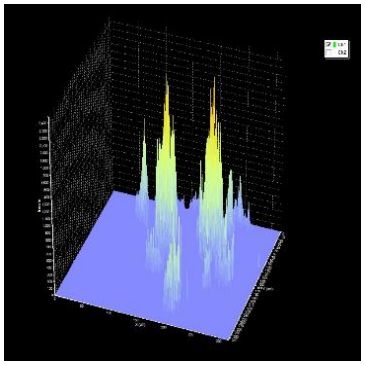	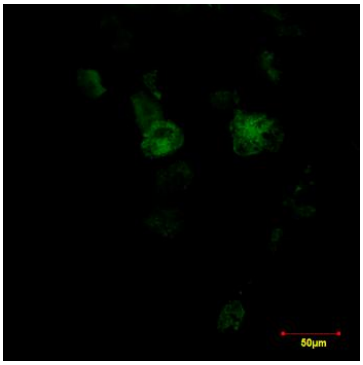

Biofilm composition under varying NaCl concentrations using FTIR

FTIR analysis provides insights into the biofilm's molecular structure and chemical composition, revealing the effect of the functional groups and molecular bonds present in the biofilm matrix at different NaCl concentrations. The FTIR spectra (Figure 5) show distinct peaks corresponding to various functional groups, with notable variations across different NaCl treatments (2%, 20%, and 40%).

At 2% NaCl, the FTIR spectrum displays a prominent broad peak between 3600 and 3200 cm^{-1}, characteristic of strong O-H stretching vibrations. This peak likely arises from water molecules and hydroxyl groups within the biofilm matrix (Rath et al. 2022; Dai et al. 2023). The intensity of this peak suggests a high water content in the biofilm, consistent with the SEM results in Table 2, where a high proportion of live cells indicated an environment conducive to microbial activity and hydration. The peak at 2900-2800 cm^{-1} corresponds to C-H stretching vibrations from alkyl groups in lipids or proteins (Ranathunga et al. 2023), indicating the presence of organic components such as fatty acids or membrane-bound proteins. A sharp peak around 1640 cm^{-1} suggests bending vibrations of H-O-H from water and potential C=O stretching from amide groups in proteins (Chatterley et al. 2022). Additionally, a broad absorption around 1200-1000 cm^{-1} is associated with C-O-C and C-O stretching in polysaccharides, reflecting the presence of carbohydrate components in the biofilm's extracellular matrix.

At 20% NaCl, the FTIR spectrum shows a broad peak at 3300-3400 cm^{-1}, indicating strong O-H stretching, potentially due to hydroxyl groups in polysaccharides or bound water molecules (Ghosh et al. 2022; Kumar et al. 2023). The presence of intermolecular hydrogen bonding is suggested by the broadness of the peak (Rath et al. 2022). Peaks at 2900-3000 cm^{-1} indicate C-H stretching, reflecting the organic

nature of the biofilm. The intense peaks at 1630-1650 cm^{-1} and 1540-1550 cm^{-1} are characteristic of protein vibrations, such as C=O stretching from amide I and N-H bending from amide II, indicating a substantial presence of protein in the biofilm matrix (Chatterley et al. 2022; Nurfitriani et al. 2022). The high intensity of protein-associated peaks at 20% NaCl correlates with the increased biovolume and protein content observed in Table 3, suggesting that moderate osmotic stress may induce enhanced biofilm production and EPS synthesis as protective responses (Dai et al. 2023).

At 40% NaCl, the spectrum displays a broad and strong absorption band between 3600-3200 cm^{-1}, similar to lower salinities but with reduced intensity, indicating a lower water content in the biofilm. The peaks around 3000-2800 cm^{-1} suggest the presence of organic compounds, but their intensity is lower than 20% NaCl, reflecting decreased organic content (Kumar et al. 2023). Sharp peaks at 1650-1550 cm^{-1} associated with C=O and N-H bending vibrations imply the continued presence of protein, albeit at lower levels (Ahmad et al. 2022; Gieroba et al. 2023). A reduction in the 1200-1000 cm^{-1} range indicates a decrease in polysaccharide content, suggesting that the biofilm matrix's composition is compromised under extreme osmotic conditions, leading to a reduction in structural components like proteins and polysaccharides (Ranathunga et al. 2023). These findings align with the SEM results in Tables 2 and 3, where cell viability, biovolume, and protein intensity decreased significantly at 40% NaCl.

Bacterial abundance dynamics under varying NaCl concentrations

The bacterial abundance data (Figure 6) depict the growth dynamics over 21 days under different NaCl conditions: A. 2% NaCl; B. 20% NaCl; and C. 40% NaCl. The growth patterns in each treatment followed a similar trajectory, starting with a lag phase from day 1 to day 3, with no significant growth being detected across all conditions. This initial phase likely reflects the period of bacterial adaptation to the new environment, where cells acclimate to osmotic conditions and initiate metabolic adjustments necessary for growth (Al Zamzami et al. 2023b).

Following the initial lag phase, bacterial abundance increased rapidly during the exponential phase (days 3-4), indicating successful adaptation and efficient nutrient utilization across all NaCl concentrations. It was followed by a stationary phase, likely due to nutrient depletion, waste accumulation, or salinity-induced stress, particularly in high-salt treatments.

Across all salinity levels, biofilm samples consistently exhibited higher bacterial abundance than planktonic counterparts, especially after day 4. It is attributed to the protective role of the Extracellular Polymeric Substance (EPS) matrix, which enhances bacterial survival by mitigating environmental stress (Sauer et al. 2022). The bacterial abundance patterns observed in water samples at day 0, day 21, and biofilm communities across all treatments showed consistent similarity. This phenomenon is likely due to the use of seawater naturally dominated by halophilic bacteria as the initial starter culture. As halophilic bacteria inherently possess robust adaptive mechanisms to hypersaline conditions, all experimental treatments ultimately exhibited parallel abundance trends despite their differing growth modes (planktonic and biofilm).

At 2% NaCl, biofilms showed the highest viable bacterial abundance, aligning with increased biovolume and protein intensity (Table 2). The low osmotic pressure supported robust microbial growth and active proliferation, as confirmed by SEM results showing the dominance of live cells, which is ideal for mildly halophilic bacteria. At 20% NaCl, bacterial abundance was also high, especially in biofilms, indicating that moderate salinity triggers adaptive stress responses, including increased EPS production.

The strengthened structure enhances cell protection and facilitates quorum sensing, allowing coordination of responses to environmental changes (Naamala et al. 2023; Kurniawan et al. 2024b; Tat 2024). Conversely, at 40% NaCl, bacterial abundance declined significantly in biofilm and planktonic forms. It correlates with reduced biovolume, lower protein content, and SEM evidence of widespread cell death, highlighting the detrimental impact of extreme osmotic stress on microbial viability and biofilm development.

Water quality parameters

pH dynamics

The 21-day pH measurements showed that pH levels varied across different NaCl concentrations, with 2% NaCl being the highest pH (alkaline) and 20% NaCl displaying the lowest pH (acidic) (Figure 7). At 2% NaCl condition, the higher pH correlated with favorable conditions for mildly halophilic bacteria, where active but moderate metabolic activity led to limited acid production and effective buffering by the biofilm's EPS. In contrast, 20% NaCl exhibited the lowest pH, reflecting high microbial abundance and metabolic activity, which produced organic acids and contributed to water acidification. For 40% NaCl, the pH was intermediate due to reduced microbial growth and lower metabolic activity, resulting in fewer acidic byproducts. This condition also showed a higher proportion of dead cells, indicating that extreme osmotic stress limited the biofilm's metabolic impact on pH.

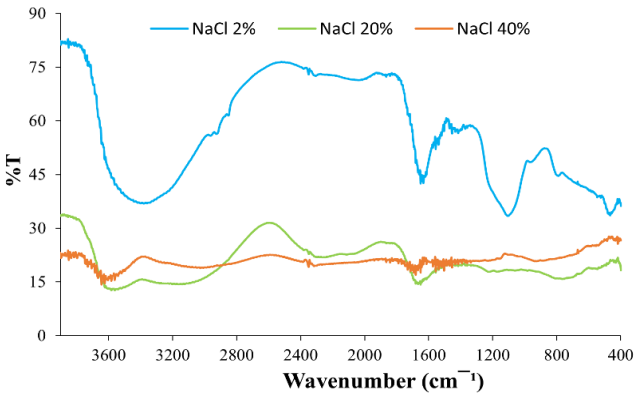

Figure 5. FTIR spectra of biofilm halophilic at different NaCl concentrations

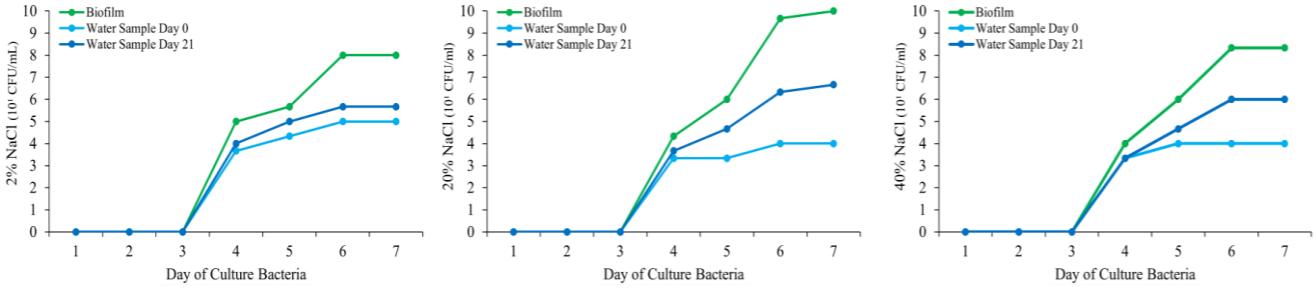

Figure 6. Abundance of bacteria. A. 2% NaCl, B. 20% NaCl, C. 40% NaCl

Dissolved oxygen dynamics

The DO levels showed a general decline across all NaCl treatments over 21 days. The highest DO was observed at 2% NaCl, where moderate microbial activity allowed balanced oxygen consumption. This treatment maintained higher DO levels due to efficient oxygen utilization without excessive metabolic demand, consistent with higher pH values (Figure 7) and greater cell viability (Table 2). In the 20% NaCl treatment, DO dropped sharply, corresponding with the highest bacterial abundance and intense metabolic activity (Figure 8). The denser biofilm matrix limited oxygen diffusion, leading to greater DO depletion. The increased oxygen consumption is aligned with lower pH levels, indicating active metabolism and acid production. At 40% NaCl, dissolved oxygen levels were at the lowest, and microbial abundance was reduced, likely attributable to elevated cellular stress and compensatory oxygen uptake by surviving microorganisms (Al Zamzami et al. 2023b). At this condition, structural integrity in the biofilm was also lower (Table 2), with limited oxygen availability and exacerbating DO depletion.

Turbidity dynamics

The data presented in Figure 9 indicate a significant increase in turbidity as NaCl concentration rises from 2% to 40%. Higher turbidity corresponds with increased suspended solids in the liquid, which can result from the higher salt concentrations. NaCl at elevated salinity induces particle aggregation, increasing the number of suspended solids and raising turbidity levels. The hygroscopic nature of NaCl also contributes to this effect, as it absorbs water and alters the physical state of particles, further enhancing turbidity (Wijnhorst et al. 2023). Moreover, the interaction between Na^+ and Cl^- ions with other particles in the solution at higher concentrations may lead to aggregates or flocs, similar to the coagulation process, where small particles combine to form larger ones (Kumar et al. 2023). The increasing turbidity observed at 40% NaCl suggests more substantial particle aggregation and higher suspended solids concentrations than the lower salinity conditions. These findings align with other results that show decreased cell viability and increased osmotic stress at higher NaCl concentrations. The combination of high turbidity and extreme salinity likely impacts the overall biofilm environment, potentially limiting light penetration and influencing microbial growth dynamics within the biofilm matrix.

Conductivity dynamics

The conductivity data (Figure 10) demonstrate an apparent increase as NaCl concentration rises from 2% to 40%. Conductivity, which measures the water's ability to conduct electricity, is directly influenced by the concentration of dissolved ions, such as Na^+ and Cl^- (Hu and Lu 2020; Gullbrekken et al. 2023). Higher salinity levels result in greater ion concentrations, which explains the increased conductivity observed at 40% NaCl compared to the lower concentrations. The highest conductivity at 40% NaCl reflects the elevated ionic strength and extensive ion dissociation in the solution, facilitating higher electrical conductivity. It aligns with the observed decrease in microbial viability and structural integrity of the biofilm under extreme salinity, suggesting that higher ion concentrations impose osmotic stress that challenges the biofilm's adaptive mechanisms. At 2% NaCl, conductivity values were the lowest, corresponding with lower ionic strength in the water. The moderate conductivity in the 20% NaCl condition reflects intermediate ionic levels, which correlate with optimal biofilm development and higher bacterial abundance in other analyses (e.g., Figure 6 for bacterial growth). The relatively stable conductivity in this condition suggests balanced ion availability that supports metabolic processes without overwhelming the microbial community.

Total dissolved solid dynamics

The TDS measurements (Figure 11) show a noticeable increase in NaCl concentrations from 2% to 40%. TDS represents the total concentration of dissolved substances, including salts, minerals, and organic matter, in water. As NaCl concentration increases, the dissolved ions, such as Na^+ and Cl^-, naturally elevate, leading to higher TDS levels. The highest TDS values observed at 40% NaCl indicate a significantly higher concentration of dissolved solids due to the substantial amount of dissolved salt. The moderate TDS levels at 20% NaCl reflect an intermediate concentration of dissolved ions, consistent with optimal biofilm growth conditions observed in other analyses, such as higher bacterial abundance and biofilm biovolume (Figure 6, Table 2). It suggests moderate salinity supports a stable ionic environment that enhances biofilm formation

and microbial activity. At 2% NaCl, the TDS values were the lowest, indicating fewer dissolved solids and a lower ionic concentration. It aligns with the lower osmotic pressure in the system, allowing for favorable microbial growth without the stress associated with high salinity.

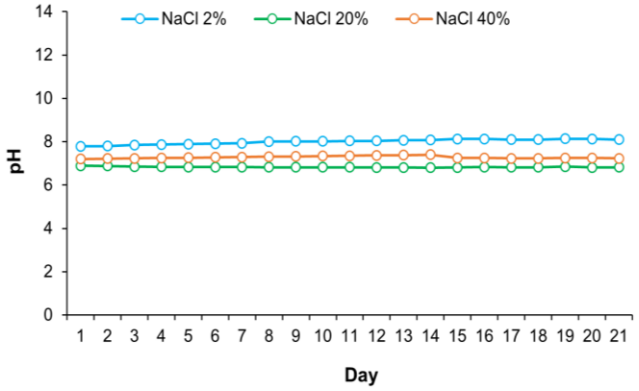

Figure 7. Water pH during the process of biofilm formation in hypersaline environments

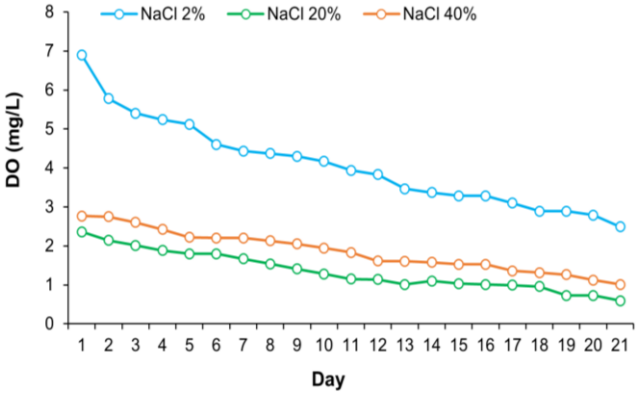

Figure 8. Dissolved Oxygen during the process of biofilm formation in hypersaline environments

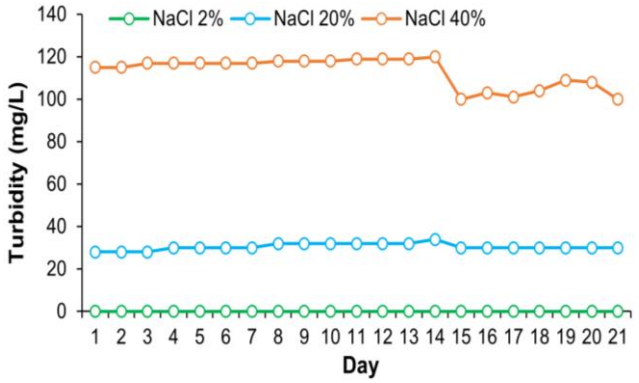

Figure 9. Water turbidity during the process of biofilm formation in hypersaline environments

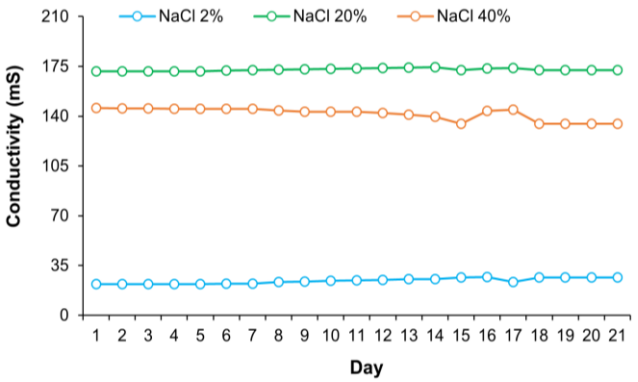

Figure 10. Conductivity of water during the process of biofilm formation in hypersaline environments

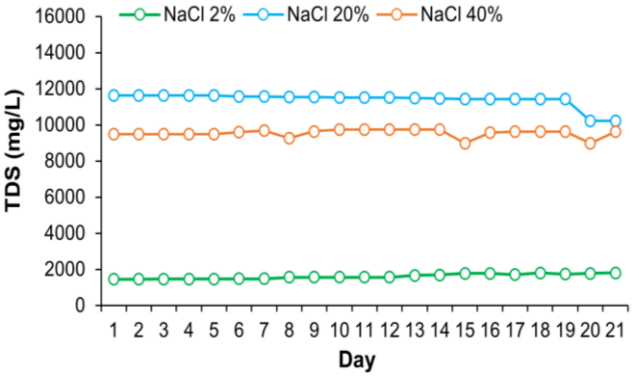

Figure 11. Total dissolved solid of water during the process of biofilm formation in hypersaline environments

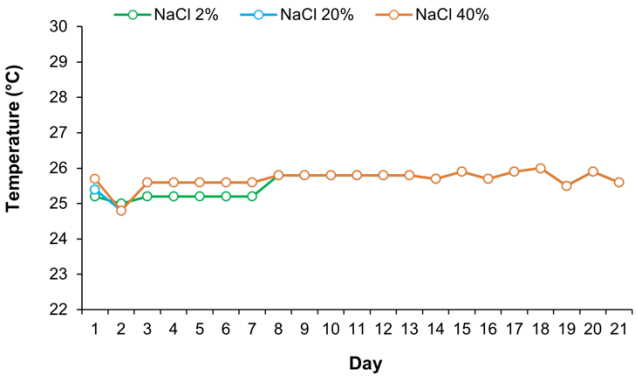

Figure 12. Water temperature during the process of biofilm formation in hypersaline environments

Temperature dynamics

The temperature data (Figure 12) indicate relatively stable readings across the 21 days for all NaCl concentrations (2%, 20%, and 40%). The stability suggests that temperature was well-controlled throughout the experiment, with no significant fluctuations that could directly impact microbial activity or biofilm formation. This controlled temperature environment ensures that any observed variations in biofilm characteristics are primarily attributable to changes in NaCl concentration rather than temperature effects. Although temperature remained constant, its influence on biofilm formation cannot be entirely disregarded, as it affects microbial metabolism and enzyme activity. The stable temperature allowed for consistent metabolic rates across treatments, enabling a more direct comparison of how different salinity levels influenced biofilm development, microbial growth, and environmental parameters like pH, DO, and TDS.

In conclusion, water quality trends (pH, DO, turbidity, conductivity, TDS, and temperature) demonstrate that environmental conditions affect halophilic biofilm formation across salinity gradients. At optimal 20% NaCl, biofilms demonstrated peak microbial abundance and biovolume, with decreased pH (indicating metabolic activity) and DO (reflecting oxygen demand). Concurrently, increased turbidity indicated robust EPS production and cellular aggregation. In extreme conditions (40% NaCl), conductivity and Total Dissolved Solids (TDS) values are elevated. This phenomenon was indicative of osmotic stress, a condition that led to a decline in microbial viability and the integrity of biofilms. The structural integrity of the biofilms was compromised, as evidenced by structural damage, minimal metabolic activity, and a significant increase in turbidity resulting from the accumulation of cellular debris. In contrast, 2% NaCl exhibited the capacity to stabilize conditions (elevated pH/DO, diminished turbidity) that fostered the development of biofilms that were less complex but still adequately performed the function of microbial respiration. These findings enhance understanding of halophilic biofilm dynamics, supporting biotechnological applications like saline wastewater bioremediation while highlighting the need for future research on molecular adaptation mechanisms and ecological roles in hypersaline environments.

ACKNOWLEDGEMENTS

The author would like to express the deepest gratitude to the Faculty of Fisheries and Marine Sciences, Brawijaya University, Malang, Indonesia and the Coastal and Marine Research Centre of Brawijaya University for the facilities and equipment that greatly assisted this research. This research was funded by the Directorate of Research and Community Services, Brawijaya University (DRPM UB) through the Basic Research (Featured) Grant (*Penelitian Dasar Unggulan*) under the grant: 00140.24/UN10.A0501/B/PT.01.03.2/2024.

REFERENCES

Ahmad HH, Nurdradjat A, Johanes H, Hariyanto AD. 2022. The FTIR investigation to characterize of functional groups in bituminous coal. Rasayan J Chem 15: 1772-1778. DOI: 10.31788/RJC.2022.1536894.

Al Zamzami IM, Kilawati Y, Ibdiah R, Kurniawan A. 2023a. Analysis of protein profile and functional groups in biofilms in the hypersaline environment. Jurnal Penelitian Pendidikan IPA 9 (12): 11351-11358. DOI: 10.29303/jppipa.v9i12.4464.

Al Zamzami IM, Kilawati Y, Pramudia Z, Susanti YAD, Kurniawan A. 2023b. Analysis of microbial abundances in biofilms and water in hypersaline environments with different NaCl levels. J Exp Life Sci 13 (2): 113-121. DOI: 10.21776/ub.jels.2023.013.02.07.

Al-Daghistani HI, Zein S, Abbas MA. 2024. Microbial communities in the Dead Sea and their potential biotechnological applications. Commun Integr Biol 17 (1): 2369782. DOI: 10.1080/19420889.2024.2369782.

Anggayasti WL, Pramudia Z, Susanti YAD, Al Zamzami IM, Moehammad KS, Wardana ING, Kurniawan A. 2025. Epilithic biofilm as a potential biomonitor for microplastics contamination in Brantas River of Malang City, Indonesia. Case Stud Chem Environ Eng 11: 101083. DOI: 10.1016/j.cscee.2024.101083.

Basotra N, Raheja R, Sharma G, Singh KA, Sharma D, Rai R, Chadha BS. 2022. Bioprospecting extremophiles for sustainable biobased industry. In: Dheeran P, Kumar S (eds). Extremophiles: General and Plant Biomass Based Biorefinery. CRC Press, Boca Raton.

Chatterley AS, Laity P, Holland C, Weidner T, Woutersen S, Giubertoni G. 2022. Broadband multidimensional spectroscopy identifies the amide II vibrations in silkworm films. Molecules 27 (19): 6275. DOI: 10.3390/molecules27196275.

Citarasu T, Thirumalaikumar E, Abinaya P, Babu MM, Uma G. 2021. Biosurfactants from halophilic origin and their potential applications. In: Inamuddin, Adetunji CO, Asiri AM (eds). Green Sustainable Process for Chemical and Environmental Engineering and Science. Microbially-Derived Biosurfactants for Improving Sustainability in Industry. Elsevier Publisher, Amsterdam. DOI: 10.1016/B978-0-12-823380-1.00019-8.

Dai F, Zhuang Q, Huang G, Deng H, Zhang X. 2023. Infrared spectrum characteristics and quantification of OH groups in coal. ACS Omega 8 (19): 17064-17076. DOI: 10.1021/acsomega.3c01336.

Ding W, Li Y, Chen M, Chen R, Tian X, Yin H, Zhang S. 2022. Structures and antitumor activities of ten new and twenty known surfactins from the deep-sea bacterium *Limimaricola* sp. SCSIO 53532. Bioorg Chem 120: 105589. DOI: 10.1016/j.bioorg.2021.105589.

Ghosh N, Roy S, Bandyopadhyay A, Mondal JA. 2022. Vibrational Raman spectroscopy of the hydration shell of ions. Liquids 3 (1): 19-39. DOI: 10.3390/liquids3010003.

Gieroba B, Kalisz G, Krysa M, Khalavka M, Przekora A. 2023. Application of vibrational spectroscopic techniques in the study of the natural polysaccharides and their cross-linking process. Intl J Mol Sci 24 (3): 2630. DOI: 10.3390/ijms24032630.

Gonzalez-Machado C, Capita R, Riesco-Peláez F, Alonso-Calleja C. 2018. Visualization and quantification of the cellular and extracellular components of *Salmonella agona* biofilms at different stages of development. PLoS One 13 (7): e0200011. DOI: 10.1371/journal.pone.0200011.

Gullbrekken Ø, Røe IT, Selbach SM, Schnell SK. 2023. Charge transport in water-NaCl electrolytes with molecular dynamics simulations. J Phys Chem B 127 (12): 2729-2738. DOI: 10.1021/acs.jpcb.2c08047.

Hu Y-S, Lu Y. 2020. The mystery of electrolyte concentration: From superhigh to ultralow. ACS Energy Lett 5 (11): 3633-3636. DOI: 10.1021/acsenergylett.0c02234.

Jurdzinski KT, Mehrshad M, Delgado LF, Deng Z, Bertilsson S, Andersson AF. 2023. Large-scale phylogenomics of aquatic bacteria reveal molecular mechanisms for adaptation to salinity. Sci Adv 9 (21): eadg2059. DOI: 10.1126/sciadv.adg2059.

Kumar H, Gaur A, Karuna MS. 2023. Synthesis of biodegradable carboxymethyl cellulose film-loaded magnesium nanoparticles. Emergent Mater 6: 561-571. DOI: 10.1007/s42247-023-00473-4.

Kurniawan A, Amin AA, Yanuar AT, Pramudia Z, Susanti YAD, Al Zamzami IM, Kurniaty R, Hakim L, Ardian G, Amenan M. 2024a. Exploring viability and innovation requirements for novel salt production: A case study of Kangen Beach, Malang Regency's South Coast, Indonesia. Cogent Soc Sci 10 (1): 2434667. DOI: 10.1080/23311886.2024.2434667.

Kurniawan A, Fukuda Y. 2023. Analysis of the electric charge properties of biofilm for the development of biofilm matrices as biosorbents for water pollutant. Energy Ecol Environ 8: 62-68. DOI: 10.1007/s40974-022-00253-6.

Kurniawan A, Pramudia Z, Susanti YAD, Al Zamzami IM, Yamamoto T. 2024b. Comparative biosorption proficiency in intact and autoclaved biofilm matrices. J Ecol Eng 25 (4): 131-141. DOI: 10.12911/22998993/183943.

Kurniawan A, Salamah LN, Winarsih W, Nurjannah N, Al Zamzami IM. 2024c. Binary biosorption of Cu (II) and Cr (VI) by naturally formed biofilm matrices. Environ Res Eng Manag 80 (3): 124-133. DOI: 10.5755/j01.erem.80.3.35773.

Kurniawan A, Syafi'i MI, Ardian G, Jaziri AA, Amin AA, Budiyanto B, Amenan M, Salamah LN, Setiawan WB. 2019. Continuously Dynamic Mixing (CDM) method and Greenhouse Salt Tunnel (GST) technology for sea salt production throughout the year. Jurnal Ilmiah Perikanan dan Kelautan 11 (2): 82-91. DOI: 10.20473/jipk.v11i2.13480.

Lyu L, Li J, Chen Y, Mai Z, Wang L, Li Q, Zhang S. 2022. Degradation potential of alkanes by diverse oil-degrading bacteria from deep-sea sediments of Haima cold seep areas, South China Sea. Front Microbiol 13: 920067. DOI: 10.3389/fmicb.2022.920067.

Mahto KU, Vandana, Priyadarshanee M, Samantaray DP, Das S. 2022. Bacterial biofilm and extracellular polymeric substances in the treatment of environmental pollutants: Beyond the protective role in survivability. J Clean Prod 379 (Part 2): 134759. DOI: 10.1016/j.jclepro.2022.134759.

Naamala J, Subramanian S, Msimbira LA, Smith DL. 2023. Effect of NaCl stress on exoproteome profiles of *Bacillus amyloliquefaciens* EB2003A and *Lactobacillus helveticus* EL2006H. Front Microbiol 14: 1206152. DOI: 10.3389/fmicb.2023.1206152.

Nurfitriani S, Arisoesilaningsih E, Nuraini Y, Handayanto E. 2022. Biofilm formation by mercury resistant bacteria from polluted soil small-scale gold mining waste. Biodiversitas 23 (2): 992-999. DOI: 10.13057/biodiv/d230242.

Oren A. 2015. Halophilic microbial communities and their environments. Curr Opin Biotechnol 33: 119-124. DOI: 10.1016/j.copbio.2015.02.005.

Orhan F, Demirci A. 2020. Salt stress mitigating potential of halotolerant/halophilic plant growth promoting. Geomicrobiol J 37 (7): 663-669. DOI: 10.1080/01490451.2020.1761911.

Perwira IY, Ulinuha D, Al Zamzami IM, Ahmad FH, Kifly MTH, Wulandari N. 2020. Environmental factors associated with decomposition of organic materials and nutrients availability in the water and sediment of Setail River, Banyuwangi, Indonesia. IOP Conf Ser: Earth Environ Sci 493: 012025. DOI: 10.1088/1755-1315/493/1/012025.

Ranathunga A, Thumanu K, Kiatponglarp W, Siriwong S, Wansuksri R, Suwannaporn P. 2023. Image mapping of biological changes and structure-function relationship during rice grain development via Synchrotron FTIR spectroscopy. Food Chem Adv 2: 100290. DOI: 10.1016/j.focha.2023.100290.

Rath S, Palit K, Das S. 2022. Variable pH and subsequent change in pCO_2 modulates the biofilm formation, synthesis of extracellular polymeric substances, and survivability of a marine bacterium *Bacillus stercoris* GST-03. Environ Res 214: 114128. DOI: 10.1016/j.envres.2022.114128.

Rieder J, Kapopoulou A, Bank C, Adrian-Kalchhauser I. 2023. Metagenomics and metabarcoding experimental choices and their impact on microbial community characterization in freshwater recirculating aquaculture systems. Environ Microbiome 18 (1): 8. DOI: 10.1186/s40793-023-00459-z.

Sarwa N, Kumari P, Meena D, Udawat P, Chaudhary NS. 2024. Alkaline proteases from haloalkaliphiles: Unveiling nature's catalysts for diverse applications. Appl Biochem Microbiol 60: 855-870. DOI: 10.1134/S0003683824603676.

Sauer K, Stoodley P, Goeres DM, Hall-Stoodley L, Burmølle M, Stewart PS, Bjarnsholt T. 2022. The biofilm life cycle: Expanding the conceptual model of biofilm formation. Nat Rev Microbiol 20 (10): 608-620. DOI: 10.1038/s41579-022-00767-0.

Shu W-S, Huang L-N. 2022. Microbial diversity in extreme environments. Nat Rev Microbiol 20: 219-235. DOI: 10.1038/s41579-021-00648-y.

Tat TQ. 2024. Isolation and identification of salt-tolerant, phosphorus-solubilizing bacterial strains from rice soil in rice-shrimp farming systems in Tien Giang Province, Vietnam. Biodiversitas 25 (10): 3868-3875. DOI: 10.13057/biodiv/d251047.

Thompson TP, Megaw J, Kelly SA, Hopps J, Gilmore BF. 2022. Microbial communities of halite deposits and other hypersaline environments. Adv Appl Microbiol 120: 1-32. DOI: 10.1016/bs.aambs.2022.06.001.

Ulinuha D, Andayani S, Hertika AMS, Kilawati Y. 2020. Estimation of bacterial number in the water, sediment and biofilm of Badek and Mewek River (Malang, Indonesia) using Plate Count and eDNA Method. Biodiversitas 21 (8): 3832-3836. DOI: 10.13057/biodiv/d210852.

Wang D, Ning Q, Deng Z, Zhang M, You J. 2022. Role of environmental stresses in elevating resistance mutations in bacteria: Phenomena and mechanisms. Environ Pollut 307: 119603. DOI: 10.1016/j.envpol.2022.119603.

Wang W, Cao Y, Li J, Lu S, Ge H, Pan S, Pan X, Wang L. 2023. The impact of osmotic stresses on the biofilm formation, immunodetection, and morphology of *Aeromonas hydrophila*. Microbiol Res 269: 127301. DOI: 10.1016/j.micres.2023.127301.

Wijnhorst R, Demmenie M, Jambon-Puillet E, Ariese F, Bonn D, Shahidzadeh N. 2023. Softness of hydrated salt crystals under deliquescence. Nat Commun 14 (1): 1090. DOI: 10.1038/s41467-023-36834-0.